



## High-Fidelity Gates in a Single Josephson Qubit

Erik Lucero,<sup>1</sup> M. Hofheinz,<sup>1</sup> M. Ansmann,<sup>1</sup> Radoslaw C. Bialczak,<sup>1</sup> N. Katz,<sup>1,2</sup> Matthew Neeley,<sup>1</sup> A. D. O'Connell,<sup>1</sup> H. Wang,<sup>1</sup> A. N. Cleland,<sup>1</sup> and John M. Martinis<sup>1,\*</sup>

<sup>1</sup>*Department of Physics, University of California at Santa Barbara, Broida Hall, Santa Barbara, California 93106, USA*

<sup>2</sup>*Racah Institute of Physics, Hebrew University of Jerusalem, Jerusalem 91904, Israel*

(Received 7 February 2008; published 16 June 2008)

We demonstrate new experimental procedures for measuring small errors in a superconducting quantum bit (qubit). By carefully separating out gate and measurement errors, we construct a complete error budget and demonstrate single qubit gate fidelities of 0.98, limited by energy relaxation. We also introduce a new metrology tool—a Ramsey interference error filter—that can measure the occupation probability of the state  $|2\rangle$ , which is outside the computational basis, down to  $10^{-4}$ , thereby confirming that our quantum system stays within the qubit manifold during single qubit logic operations.

DOI: [10.1103/PhysRevLett.100.247001](https://doi.org/10.1103/PhysRevLett.100.247001)

PACS numbers: 85.25.Cp, 03.67.Lx, 03.67.Pp, 74.50.+r

The immense computational power of a quantum computer comes with a cost—the fragility of entangled quantum states from coherence loss. Although decoherence is present in all qubit implementations, the effect of the resulting logic errors can be overcome by using error-correcting codes, provided that gate errors fall below a fault-tolerance threshold [1–5]. This threshold depends on system architecture and the specific form of decoherence, but is likely to be in the  $\sim 10^{-4}$  range [1]. The measurement of gate fidelity in this range is thus a critical step in implementing fault-tolerant quantum computation. To date, high-fidelity single and multiple-qubit logic gates have only been demonstrated in ion traps [6,7]. Solid-state systems such as Josephson qubits [8–23], which have the potential advantage of scalability, have not achieved equivalent fidelities. Here, we measure the fidelity of a single qubit gate for a Josephson phase qubit, demonstrating substantial progress towards this goal. Using the new metrological technique of “Ramsey filtering”, we also show how one important error process can be measured and reduced to a magnitude of  $10^{-4}$ .

Coherence is typically quantified through the energy decay time  $T_1$  and coherence time  $T_2$  (that includes dephasing) obtained from a Ramsey fringe experiment. The fidelity of a gate operation is then computed as the ratio of the gate time to coherence time. We note, however, that such an analysis assumes no loss in fidelity during a logic gate operation when the quantum state is changed, and thus it more properly corresponds to the fidelity of a memory operation. In addition, these coherence times are typically determined by the relative decay in an experimental signal assumed to be proportional to the state probability, thus ignoring any fidelity loss that might be constant in time. A full measurement of gate fidelity should include gate errors that are determined via probabilities with an absolute calibration.

To illustrate the importance of these issues, we note that many experimental systems use qubit states  $|0\rangle$  and  $|1\rangle$ , often the ground and first excited states, chosen from a

larger set of basis states [24]. This encoding does not preclude unwanted excitations to other available states in the basis. For example, excitations to the next higher energy state  $|2\rangle$  are not necessarily small and correspond to gate errors that may not be included in standard measurements of  $T_1$  and  $T_2$ .

In the experiments described here we used a superconducting phase qubit, where the superconducting phase difference  $\delta$  in a Josephson junction (with critical current  $I_0$ ) serves as the quantum variable. When biased close to the critical current, the junction and its loop inductance  $L$  generate a cubic potential where the two lowest energy eigenstates  $|0\rangle$  and  $|1\rangle$  have a transition frequency  $\omega_{10}/2\pi \sim 6.75$  GHz [see Fig. 1(a)]. This frequency can be adjusted by  $\sim 30\%$  using the junction bias current. The circuit layout and operation have been described previously [19,25].

Single qubit logic operations, corresponding to rotations about the  $x$ ,  $y$ , and  $z$  axes of the Bloch sphere, are generated as follows: Rotations about the  $z$  axis are produced from current pulses on the qubit bias line that adiabatically change the qubit frequency, leading to phase accumulation between the states  $|0\rangle$  and  $|1\rangle$  [26]. Rotations about any axis in the  $x$ - $y$  plane are produced by microwave pulses resonant with the qubit transition frequency. The phase of the microwave pulses defines the orientation of the rotation axis in the  $x$ - $y$  plane, and the pulse duration and amplitude control the rotation angle.

We perform single shot readout of the phase qubit by applying a fast ( $\sim 1$  ns rise time) current pulse  $I_z$ . This fast pulse lowers the barrier height and increases the tunneling probability of the  $|1\rangle$  state [Fig. 1(b)]. Once tunneled, the state quickly decays into an external lower energy state that can be easily distinguished from the untunneled state  $|0\rangle$  using an on-chip superconducting quantum interference device (SQUID) [20].

Nonideal behavior of the qubit can arise from errors either in the logic gate or in the state measurement. The measurement errors can be accounted for by thoroughly

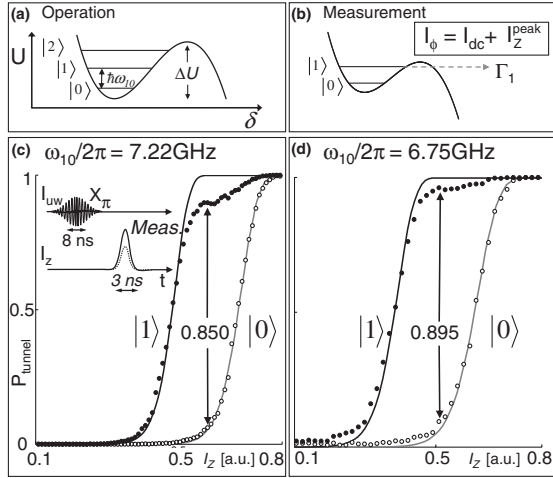


FIG. 1. Qubit operation and state measurement. (a) The potential energy  $U$  of a Josephson phase qubit versus junction phase  $\delta$ . The qubit is formed from the two lowest eigenstates  $|0\rangle$  and  $|1\rangle$ , with a transition frequency  $\omega_{10}/2\pi \approx 6.75$  GHz that can be adjusted by varying the dc bias  $I_\phi = I_{dc} + I_z$ . (b) A measurement pulse lowers the energy barrier  $\Delta U$ , increasing the  $|1\rangle$  state tunneling probability. (c) Tunneling probability versus measurement amplitude  $I_z$  for the qubit in the states  $|0\rangle$  (open circles) and  $|1\rangle$  (closed circles) at qubit frequency  $\omega_{10}/2\pi = 7.22$  GHz. Fits are shown by the solid lines. (d) Data as for C but with a larger current bias,  $I_{dc}$  giving a smaller qubit transition frequency  $\omega_{10}/2\pi = 6.75$  GHz. The visibility between states  $|0\rangle$  and  $|1\rangle$  is 0.85 and 0.895 for data in (c) and (d), respectively. The difference is directly attributed to coupling to a TLS located at 7.05 GHz, as observed with spectroscopy. The inset illustrates the pulse sequence. The  $|1\rangle$  state is prepared by applying a shaped microwave pulse for  $\tau = 8$  ns, with amplitude chosen to generate a  $\pi$  rotation. For the  $|0\rangle$  state we apply no microwaves. After state preparation, the current  $I_z$  is pulsed to measure the qubit state.

understanding their physical mechanisms. In Josephson phase qubits, measurement fidelities below unity are due to stray tunneling of the  $|0\rangle$  state, the  $|1\rangle$  state leaking energy to spurious two-level states (TLS) [27], and  $T_1$  relaxation. To quantitatively confirm TLS effects as measurement errors, we determined the measurement fidelity above and below a large TLS splitting at 7.05 GHz [28], as shown in Figs. 1(c) and 1(d). For each data set, the tunneling probability of the ground state  $|0\rangle$  is determined versus measurement pulse amplitude  $I_z$ . The  $X$  pulse is then calibrated for a  $\pi$ -rotation to give maximum probability of the  $|1\rangle$  state, and the  $|1\rangle$  state probability  $P_1$  is determined versus  $I_z$ . After this calibration,  $I_z$  is chosen to give maximum visibility, which is displayed in each figure by an arrow.

Theoretical predictions for the tunneling probabilities are given by the solid black and gray lines in Figs. 1(c) and 1(d). The  $|0\rangle$  state is misidentified as a  $|1\rangle$  state with a probability of 0.034. This error is consistent with theory, and corresponds to stray tunneling events during measure-

ment [27]. At  $\omega_{10}/2\pi = 6.75$  GHz the  $|1\rangle$  state is misidentified as the  $|0\rangle$  state with a probability of 0.071, but at a higher qubit frequency,  $\omega_{10}/2\pi = 7.22$  GHz this error increases to 0.116. The increase in measurement error with qubit frequency is attributed to a TLS located between these two frequencies. With a measurement of the TLS splitting using spectroscopy (see supplemental data in [28]), we predict a  $|1\rangle$  state population decrease of 0.045, a value consistent with our data. The remaining measurement error is accounted for with an error budget of 0.010 for  $T_1$  decay, 0.050 for coupling to other sparse TLS (below 6.75 GHz), and 0.011 for no tunneling of the  $|1\rangle$  state during measurement.

With good agreement between experiment and theory, we can reliably account for measurement errors in our data. Because the error for the  $|0\rangle$  state—due solely to stray tunneling—is simpler and less dependent on systematics, we choose to perform logic gate experiments that bring the final state close to  $|0\rangle$ , thus reducing uncertainties due to state measurement.

The fidelity of a gate is determined by applying two  $\pi$ -pulses that produce the transitions  $|0\rangle \rightarrow |1\rangle \rightarrow |0\rangle$ , and then measuring the state of the qubit. A  $\pi$ -pulse represents the maximum rotation of a single qubit operation and thus gives a measure of the maximum error for a gate. Both microwave  $\pi$ -pulses were designed to have Gaussian envelopes [28], with a duration 8 ns full width at half maximum (FWHM). The correct sequential operation of this gate is checked by testing whether the probability for the final state is independent of the phase  $\Theta$  between the two microwave pulses, as illustrated in Fig. 2(a). In Figs. 2(b) and 2(c) the experimental (theoretical) state tomography data are shown as a function of  $\Theta$  and microwave detuning  $\Delta$  from the qubit transition frequency  $\omega_{10}/2\pi$ . The experimental data are in excellent correspondence with theoretical predictions. On resonance ( $\Delta = 0$ ), the phase  $\Theta$  has no effect, as expected, which demonstrates that the two pulses are calibrated properly as  $\pi$ -pulses.

Gate error is directly measured by repeating this experiment with variable time separation  $t_{\text{sep}}$  between the two  $\pi$ -pulses, as shown in Fig. 2(d). The gate error grows with increasing time  $t_{\text{sep}} > 9$  ns because the  $|1\rangle$  state decays, and the error has a slope consistent with separate measurements of  $T_1$  indicating the errors from each pulse are uncorrelated. The error also increases at small times due to the overlap of the two Gaussian microwave pulses. The horizontal dashed line indicates  $P_1 = 0.034$  taken without the application of microwaves; the difference between the data and the dashed line is the gate error. When the pulses are separated by a time  $t_{\text{sep}} = 12$  ns, we find an error  $\Delta P_1 = 0.04$ . Since two gate operations are used for this protocol, the fidelity for a single gate operation is 0.98 [29].

Initial experiments did not reach this level of performance. We only achieved high-fidelity gates by using carefully shaped microwave pulses [28], to minimize excitation

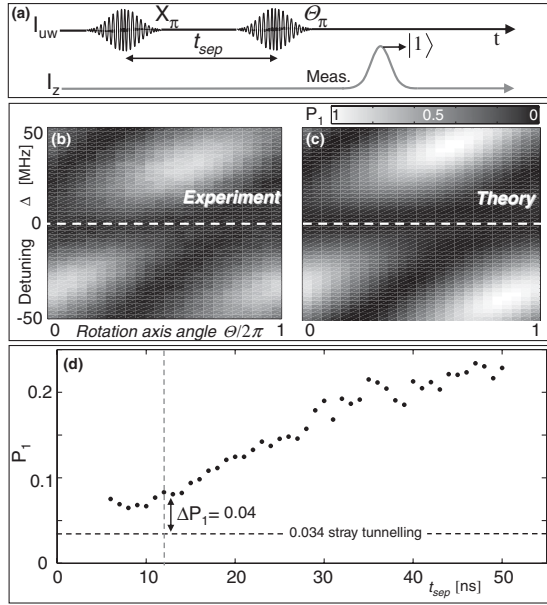


FIG. 2. Measurement of a high-fidelity gate. (a) The pulse sequence consists of two 8 ns Gaussian-shaped  $\pi$ -pulses, separated in time by  $t_{\text{sep}}$ , followed by a measure pulse  $I_z$ . The first  $\pi$ -pulse defines the rotation axes; by convention this is the  $x$  axis. For the second pulse, which is delayed by  $t_{\text{sep}}$ , we sweep the rotation axis angle  $\Theta$  by changing the phase of the microwaves. By adding a radio frequency signal (0–50 MHz) to the carrier wave we shift the microwaves away from the qubit frequency (a technique known as sideband mixing) [28]. This sequence ideally returns the qubit to the  $|0\rangle$  state. (b) Gray scale plot of measured  $|1\rangle$  state probability  $P_1$  versus detuning  $\Delta$  and phase  $\Theta$  with  $t_{\text{sep}} = 12$  ns and (c) quantum simulation. On resonance, the phase  $\Theta$  does not change  $P_1$ , as expected. (d) Plot of  $P_1$  versus  $t_{\text{sep}}$ . Measurement error of the  $|0\rangle$  state is 0.034, as obtained by performing the experiment with no microwaves. The difference between the data and this stray tunneling is 0.04 at  $t_{\text{sep}} = 12$  ns, corresponding to an error of magnitude 0.02 for each  $\pi$ -pulse, and a single qubit gate fidelity of 0.98.

of the  $|2\rangle$  state [30]. There is a tradeoff between using a fast pulse for small  $T_1$  errors, or a slow pulse for small Fourier amplitude at the  $|1\rangle \rightarrow |2\rangle$  transition frequency, as illustrated in the inset of Fig. 4. The measurement of this error is explicitly shown in Fig. 3(a), where  $P_{\text{tunnel}}$  is plotted versus  $I_z$  for a single  $\pi$ -pulse using 4, 5, and 8 ns FWHM Gaussian pulses. Excitation to the  $|2\rangle$  state produces a shoulder in  $P_{\text{tunnel}}$  at a value of measurement current  $I_z$  below the rise from the  $|1\rangle$  state, as indicated by the arrow. This probability is plotted versus Gaussian width  $\tau$  in Fig. 4 and shows that this error decreases with increasing pulse width, as expected. Errors become difficult to measure below  $\sim 0.01$  because of stray tunneling of the  $|1\rangle$  state.

The  $|2\rangle$  state error may be measured with much greater sensitivity by recognizing that excitation to the  $|2\rangle$  state is a coherent quantum process. Using a two-pulse sequence

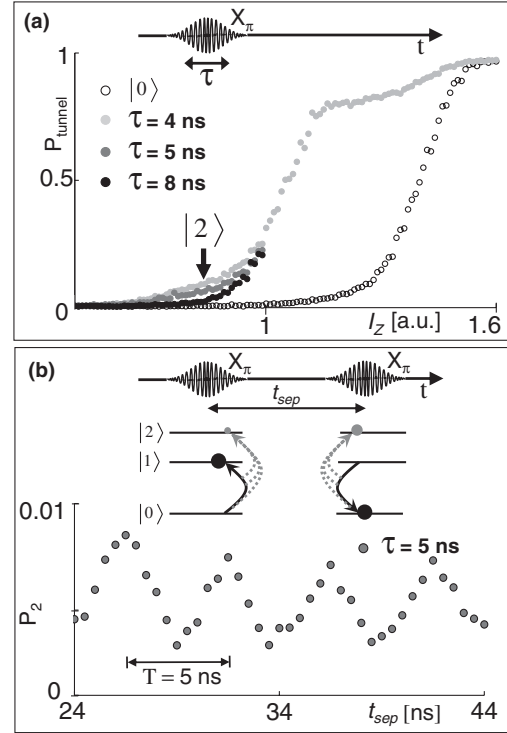


FIG. 3. Ramsey interference error filter. (a) For a single-pulse sequence, plot of tunneling probability  $P_{\text{tunnel}}$  versus  $I_z$  for  $|0\rangle$  and  $|1\rangle$  state (gray) for  $\tau = 4, 5,$  and 8 ns FWHM Gaussian-shaped  $X_\pi$ -pulses. (b) For two-pulse sequence plot of  $|2\rangle$  state probability  $P_2$  vs  $t_{\text{sep}}$  for  $\tau = 5$  ns. The two  $X_\pi$ -pulses are followed by a measure pulse with an amplitude calibrated to tunnel only the  $|2\rangle$  state. During the first  $X_\pi$ -pulse both of the states  $|1\rangle$  and  $|2\rangle$  are excited. The second  $X_\pi$ -pulse causes the coherent beating of the  $|2\rangle$  state. The amplitude of the oscillation is 4 times the error probability, whereas the beat frequency  $1/T = 1/(5 \text{ ns})$  corresponds to the qubit nonlinearity  $(\omega_{10} - \omega_{21})/2\pi$ . The insets in (a) and (b) illustrate the microwave control pulses; (b) also depicts the three-level system and the unwanted transitions to the  $|2\rangle$  state.

with variable time delay as illustrated in the inset of Fig. 3(b), a Ramsey fringe may be set up between the transitions to the  $|2\rangle$  state from the two pulses. We plot in Fig. 3(b) the  $|2\rangle$  state probability  $P_2$  versus pulse delay time  $t_{\text{sep}}$ . Since the periodic oscillation is due to coherent interference between the two pulses, the magnitude of this oscillation is 4 times the probability of exciting the  $|2\rangle$  state for a single pulse. More importantly, the “up-conversion” of a constant error to an oscillation allows a determination of the amplitude with fewer systematic errors; this error can now be reliably measured down to  $10^{-4}$  using this Ramsey filter. The oscillation frequency matches the beat frequency  $(\omega_{10} - \omega_{21})/2\pi$  measured via spectroscopy [28], and represents a further check of this measurement technique.

The  $|2\rangle$  state errors determined in this manner are also plotted in Fig. 4. For Gaussian pulses with width 4 and 5 ns,

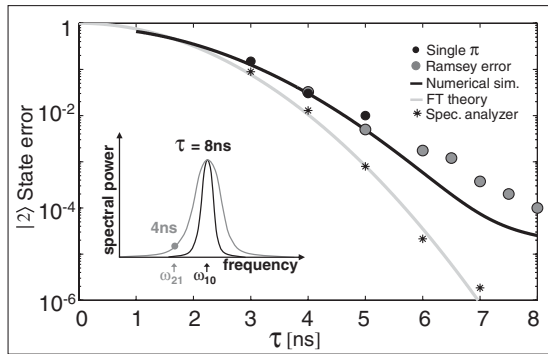


FIG. 4. Error from  $|2\rangle$  state occupation, measured at a magnitude of  $10^{-4}$ . (a) Plot of  $|2\rangle$  state error versus Gaussian pulse width for both single  $\pi$ -pulses (black circles) and Ramsey error (gray circles) data. The 8 ns FWHM Gaussian produces a  $|2\rangle$  probability of  $10^{-4}$ . The solid line is the quantum prediction obtained from numerical simulation. Spectrum analyzer data for the Gaussian-shaped pulses (asterisks) are also plotted with the Fourier-transform theory curve (solid gray line). The inset illustrates that a 4 ns pulse produces a significant amount of spectral power at  $\omega_{21}/2\pi$ .

the data from the two methods give a consistent error probability. The error drops exponentially with increasing pulse width, reaching the value  $10^{-4}$  at 8 ns. A simple Fourier-transform prediction [30] is plotted as a solid gray line, which is computed from the power spectrum of the Gaussian pulse at frequency  $\omega_{21}$ , normalized to the power at frequency  $\omega_{10}$ . The asterisks are a measurement of this normalized power taken from the actual control pulses; this simple comparison is an excellent check on the shaping of the microwave pulses as we have found that large spectral leakage gives large qubit error. The solid black line is a prediction of the error obtained from numerical calculations [30], which shows good agreement with the data.

In conclusion, we have demonstrated for single qubits an absolute gate fidelity of 0.98, the highest demonstrated in any solid-state system to date. This level of performance was achieved through careful shaping of the microwave control signals. A new metrology tool, Ramsey error filtering, has been introduced, which uses the coherence of an error process for more accurate measurement. We have demonstrated that the probability of the  $|2\rangle$  state in our system can be reduced down to  $10^{-4}$  and that our quantum system remains in the qubit manifold during our single qubit operations. These measurements further demonstrate that superconducting qubits are a leading candidate for a solid-state quantum computer.

Devices were made at the UCSB and Cornell Nanofabrication Facilities, a part of the NSF-funded National

Nanotechnology Infrastructure Network. This work was supported by ARDA under Grant No. W911NF-04-1-0204 and NSF under Grant No. CCF-0507227.

\*martinis@physics.ucsb.edu

- [1] E. Knill, *Nature (London)* **434**, 39 (2005).
- [2] A. M. Steane, *Nature (London)* **399**, 124 (1999).
- [3] E. Knill, R. Laflamme, and W. H. Zurek, *Nature, Science* **279**, 342 (1998).
- [4] D. Gottesman, *Phys. Rev. A* **57**, 127 (1998).
- [5] D. P. DiVincenzo and P. W. Shor, *Phys. Rev. Lett.* **77**, 3260 (1996).
- [6] D. Leibfried *et al.*, *Nature (London)* **422**, 412 (2003).
- [7] J. Chiaverini *et al.*, *Nature (London)* **432**, 602 (2004).
- [8] M. H. Devoret and J. M. Martinis, *Quant. Info. Proc.* **3**, 163 (2004).
- [9] J. Q. You and F. Nori, *Phys. Today* **58**, 42 (2005).
- [10] V. Bouchiat, D. Vion, P. Joyez, D. Esteve, and M. H. Devoret, *Phys. Scr.* **T76**, 165 (1998).
- [11] Y. Nakamura, Y. A. Pashkin, and J. S. Tsai, *Nature (London)* **398**, 786 (1999).
- [12] D. Vion *et al.*, *Science* **296**, 886 (2002).
- [13] I. Chiorescu, Y. Nakamura, C. J. P. M. Harmans, and J. E. Mooij, *Science* **299**, 1869 (2003).
- [14] Y. Makhlin, G. Schön, and A. Schnirman, *Rev. Mod. Phys.* **73**, 357 (2001).
- [15] M. Sillanpää, J. I. Park, and R. W. Simmonds, *Nature (London)* **449**, 438 (2007).
- [16] J. Majer *et al.*, *Nature (London)* **449**, 443 (2007).
- [17] J. H. Plantenberg, P. C. de Groot, C. J. P. M. Harmans, and J. E. Mooij, *Nature (London)* **447**, 836 (2007).
- [18] A. O. Niskanen, K. Harrabi, F. Yoshihara, Y. Nakamura, S. Lloyd, and J. S. Tsai, *Science* **316**, 723 (2007).
- [19] M. Steffen *et al.*, *Science* **313**, 1423 (2006).
- [20] J. M. Martinis, S. Nam, J. Aumentado, and C. Urbina, *Phys. Rev. Lett.* **89**, 117901 (2002).
- [21] A. Wallraff *et al.*, *Phys. Rev. Lett.* **95**, 060501 (2005).
- [22] T. Duty, D. Gunnarsson, K. Bladh, and P. Delsing, *Phys. Rev. B* **69**, 140503 (2004).
- [23] O. Astafiev, Yu. A. Pashkin, T. Yamamoto, Y. Nakamura, and J. S. Tsai, *Phys. Rev. B* **69**, 180507 (2004).
- [24] M. A. Nielsen and I. L. Chuang, *Quantum Computation and Quantum Information* (Cambridge University Press, Cambridge, England, 2000).
- [25] N. Katz *et al.*, *Science* **312**, 1498 (2006).
- [26] M. Steffen *et al.*, *Phys. Rev. Lett.* **97**, 050502 (2006).
- [27] K. B. Cooper *et al.*, *Phys. Rev. Lett.* **93**, 180401 (2004).
- [28] E. Lucero *et al.*, arXiv:0802.0903v1 [Phys. Rev. Lett. (to be published)].
- [29] We note that because of the short duration of these experiments, the coherence was not limited by  $T_2 \approx 120$  ns.
- [30] M. Steffen, J. M. Martinis, and I. L. Chuang, *Phys. Rev. B* **68**, 224518 (2003).